# *In Vitro* Visualization and Quantification of Oleic Acid Induced Changes in Transdermal Transport Using Two-Photon Fluorescence Microscopy

Betty Yu, Chen-Yuan Dong,* Peter T. C. So,* Daniel Blankschtein, and Robert Langer
Departments of Chemical Engineering and *Mechanical Engineering, Massachusetts Institute of Technology, Cambridge, Massachusetts, U.S.A.

**In a novel application of two-photon scanning fluorescence microscopy, three-dimensional spatial distributions of the hydrophilic and hydrophobic fluorescent probes, sulforhodamine B and rhodamine B hexyl ester, in excised full-thickness human cadaver skin were visualized and quantified. Both sulforhodamine B and rhodamine B hexyl ester were observed to lie primarily in the lipid multilamellae region surrounding the corneocytes within the stratum corneum. From the two-photon scanning fluorescence microscopy scans, the changes in the concentration gradient and the vehicle to skin partition coefficient of each probe induced by the oleic acid enhancer action were calculated relative to the control sample (not exposed to oleic acid), and subsequently applied to theoretically derived mathematical expressions of transdermal transport to quantitatively characterize the oleic acid-induced relative changes in the skin diffusion coefficient and the skin barrier diffusion length of the permeant. For the hydrophobic probe rhodamine B hexyl ester, the permeability enhancement was primarily driven by an increase in the vehicle to skin partition coefficient, leading to an increase in the steepness of the concentration gradient across the skin. The primary oleic acid-induced changes in the transport properties of the hydrophilic probe sulforhodamine B included increases in the vehicle to skin partition coefficient and the skin diffusion coefficient. These findings utilizing the two-photon scanning fluorescence microscopy methodology and data analysis described here demonstrate that, in addition to providing three-dimensional images that clearly delineate probe distributions in the direction of increasing skin depth, the subsequent quantification of these images provides additional important insight into the mechanistic changes in transdermal transport underlying the visualized changes in probe distributions across the skin.** ***Key words: chemical enhancement mechanism/excised human skin/fluorescent probe distribution/oleic acid/two-photon scanning fluorescence microscopy. J Invest Dermatol 117:16–25, 2001***

As a noninvasive alternative to more traditional methods of drug delivery, including oral and subcutaneous administration, transdermal drug delivery offers the advantages of patient compliance and elimination of first-pass drug metabolism (Finnin and Morgan, 1999). The inherent barrier properties of the stratum corneum (SC), the outermost layer of the skin, limits transdermal delivery to molecules that are hydrophobic and have low molecular weight (Guy, 1996). Whereas the ordered configuration of the lipid multilamellae that comprise the continuous phase of the SC creates a barrier to drug penetration (Scheuplein and Blank, 1971; Potts and Francoeur, 1991), the affinity of small hydrophobic molecules for the "oily" environment of the bilayer hydrocarbon tail region enables the transdermal delivery of drugs such as scopolamine, clonidine, nitroglycerine, estradiol, fetanyl, and nicotine (Cullander and Guy, 1992; Schaefer and Redelmeier, 1996).

The pharmaceutical relevance of many molecules, such as peptides, proteins, and other large hydrophilic molecules, which are excluded from the category of small hydrophobic molecules, has stimulated the investigation of permeability enhancement methods, such as, the application of chemical compounds to the skin to reversibly alter its resistance to drug transport (Golden *et al*, 1987; Francoeur *et al*, 1990; Naik *et al*, 1995; Yoneto *et al*, 1995; Johnson *et al*, 1996b; Peck *et al*, 1998). A description and understanding of the processes involved in chemically enhanced transdermal drug transport would enable the rational design of drug-chemical enhancer formulations, an otherwise time consuming and costly process.

Experimental techniques utilized in mechanistic studies of chemically induced transdermal drug permeability enhancement have included Fourier transform infrared spectroscopy, differential scanning calorimetry, and nuclear magnetic resonance spectroscopy (Schaefer and Redelmeier, 1996). For oleic acid, a well-known chemical enhancer, these techniques have been helpful in identifying the mode of chemical enhancer action as a fluidization of the lipid multilamellae which form the continuous phase of the SC (Francoeur *et al*, 1990; Schaefer

Manuscript received October 19, 2000; revised January 5, 2001; accepted for publication February 19, 2001.

Reprint requests to: Dr. Daniel Blankschtein, Department of Chemical Engineering, Room 66-444, Massachusetts Institute of Technology, 77 Massachusetts Avenue, Cambridge, MA 02139-4307. Email: dblank@mit.edu

Abbreviations: RBHE, rhodamine B hexyl ester perchlorate; SAIP, sample average intensity profile; SC, stratum corneum; SRB, sulforhodamine B; SSDP, spatial distribution profile; TPM, two-photon scanning fluorescence microscopy; VE, viable epidermis.

and Redelmeier, 1996). The correlation found between increased transdermal drug flux and increased lipid fluidity strongly suggests that oleic acid alters the packing structure of the SC lipids to increase lipid fluidity and reduce skin resistance to drug transport (Golden *et al*, 1987). Furthermore, the mechanism of oleic acid chemical enhancer action has been associated with the formation of phase-separated oleic acid domains in the SC multilamellar lipids (Ongpipattanakul *et al*, 1991). Whereas the above-mentioned studies (Golden *et al*, 1987; Francoeur *et al*, 1990; Schaefer and Redelmeier, 1996) have clearly elucidated the role of oleic acid in altering SC lipid ordering, the changes in the microscale transport properties of the permeant, including the vehicle to skin partition coefficient, the skin diffusion coefficient, and the skin barrier diffusion length, that underlie the experimentally measured increases in the transdermal permeability of the permeant, remain to be clarified.

Laser scanning confocal fluorescence microscopy has been utilized to visualize hydrophobic and hydrophilic fluorescent probe spatial distributions across the skin (Turner and Guy, 1997; Kuijk-Meuwissen *et al*, 1998); however, three-dimensional imaging using this technique is limited by increased light scattering within the medium. In laser scanning confocal fluorescence microscopy, the fluorescent probe penetration is, therefore, often imaged by sectioning skin samples perpendicular to the skin surface such that the field of view captures the fluorescent probe distribution from the SC to the dermis all in one plane. Because skin sample sections often undergo exposure to chemicals and mechanical forces in the curing, setting, and sectioning stages of the sample preparation procedure, the presence of artifacts in the final sample remains a potential risk.

As a noninvasive method for directly visualizing the skin structural features, TPM has been successfully used to image *in vivo* human skin (Masters *et al*, 1998). More recently, TPM has been utilized to visualize *in vitro* permeant spatial distributions across human cadaver skin.[1–3] In TPM, tight focusing in a laser scanning microscope, combined with a femtosecond pulsed laser, enables a dye molecule to simultaneously absorb two long-wavelength photons to reach its excited state (Denk *et al*, 1990). The quadratic dependence of the excitation probability results in greater three-dimensional depth discrimination. The long-wavelength photon source used in TPM allows deeper light penetration into media with a high degree of scattering (Denk *et al*, 1995; Diaspro, 1999; Soeller and Cannell, 1999), thus making it well suited for imaging the skin (Masters *et al*, 1998).

Other attributes of TPM include its use of a large area signal detector that maximizes the photon collection efficiency, and the localization of the excitation volume to the focal region, which results in minimized photodamage and photobleaching (Masters *et al*, 1997; Periasamy *et al*, 1999).

Despite the application of TPM to visualize probe distributions in the skin (Grewal *et al* 2000), to date, TPM scans of fluorescent probe distributions in the skin have not been rigorously analyzed to characterize quantitatively the changes in the transdermal transport properties resulting from chemical enhancer action. The structural complexity of the SC (described below) poses significant challenges to the quantitative analysis of average probe transport properties in the skin. This analysis relies on an accurate assessment of the fluorescent probe concentration distributions throughout the skin depth. To demonstrate the quantitative analysis methodology described below in detail, the SC was treated as a membrane in which the corneocytes and lipid multilamellae are collectively considered in the quantification of the fluorescent probe distributions in the SC. This approach, in which the corneocytes were not excluded from the analysis of transdermal permeant transport, has been commonly employed by other researchers (Mak *et al*, 1990; Naik *et al*, 1995; Pirot *et al*, 1997). Hence, the ensuing description of the TPM methodology utilized in the transdermal transport studies and the quantification of the changes detected in the microscale transport properties relative to the control case, introduce, for the first time, the novel application of TPM to this *in vitro* model skin system to elucidate the mechanism of chemical enhancer action.

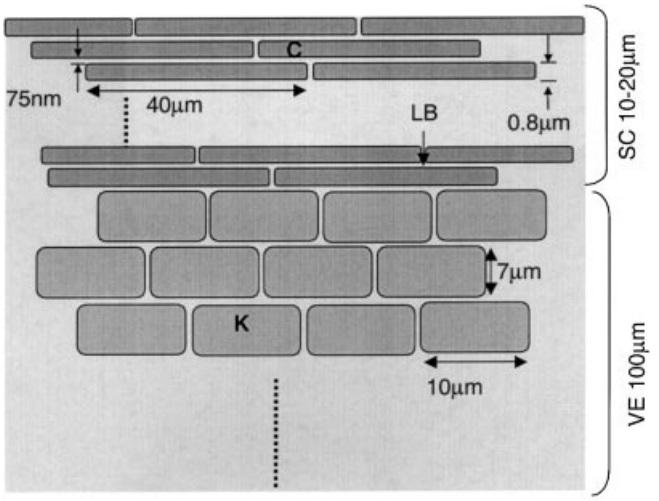


**Figure 1. Schematic illustration of the brick and mortar model of the SC, including the VE.** The corneocytes (C) and keratinocytes (K) are represented by the brick-like structures in the continuous phase of the lipid bilayer lamellae (LB) that comprise the intercellular space. In the SC—the first 10–20 μm of the skin—corneocytes have estimated dimensions of 40 μm in diameter and 0.8 μm in thickness, whereas the intercellular space thickness is estimated to be 75 nm. The keratinocytes (10 μm in diameter) in the VE undergo compression (7–0.8 μm) as they differentiate and migrate to the SC to form the corneocytes.

In the studies reported here, three-dimensional images of fluorescent probe spatial distributions across full-thickness human cadaver skin were constructed utilizing TPM data. Oleic acid-induced changes in the probe concentration gradient, as well as in the microtransport properties of the probe, including the skin diffusion coefficient, the skin barrier diffusion length, and the vehicle to skin partition coefficient, all of which influence the experimentally measured permeability of the probe across the skin, were quantified relative to the control case (without oleic acid) based on a theoretical analysis of these three- dimensional images to shed light on the mechanisms of chemically enhanced transdermal transport.

The SC—the outermost 10–20 μm layer of the skin—is the primary barrier to transdermal drug transport (Bommannan *et al*, 1990), and consists of corneocytes embedded in a continuous phase of lipid multilamellae (LB), as depicted in the schematic illustration of the brick and mortar model of the SC including the viable epidermis (VE) shown in **Fig 1**. The two-photon microscopy images discussed below will highlight permeant diffusion across the SC and a portion of the underlying VE.

The steady-state flux, J, of a permeant across the SC membrane in the absence of convective solvent flow is

[1]Yu B, Dong CY, So PTC, Mitragotri S, Blankschtein D, Langer R: Visualization and quantification of transdermal chemical enhancement using two-photon microscopy *Proceedings of the International Symposium on Controlled Release Bioactive Materials*. Controlled Release Society. 26, 1999 (Abstr. 312)

[2]Yu B, Dong CY, So PTC, Mitragotri S, Blankschtein D, Langer R: Two-photon imaging of transdermal transport processes. *Perspect Percutan Penetration* 7a:40, 2000 (Abstr.)

[3]Yu B, Dong CY, So PTC, Blankschtein D, Langer R: Examination of transdermal transport processes in excised human skin using two-photon microscopy. *Proceedings of the International Symposium on Controlled Release Bioactive Materials*. Controlled Release Society. 27, 2000 (Abstr. 7414)

commonly described using the one dimensional Fick's First Law of diffusion, namely,

$$J = -D\frac{dC}{dz} \tag{1}$$

where D is the effective permeant diffusion coefficient in the membrane, and dC/dz is the concentration gradient in the z-direction, or the direction of increasing SC depth (Peck *et al*, 1996; Pugh *et al*, 1998). From Eqn 1, changes in the permeant flux are driven by changes in two microtransport properties, D and dC/dz. Additional transport properties that contribute to the experimentally measured permeant skin permeability include the permeant vehicle to skin partition coefficient, K, and the skin barrier diffusion length, l. As discussed later, the skin barrier diffusion length, l, represents the thickness of the skin region over which the greatest barrier to permeant transdermal transport is exhibited. In discussions of percutaneous absorption, in which a constant donor solution concentration and a zero concentration receiver solution were assumed, the mathematical models derived for transdermal transport yield expressions for diffusion in one dimension (Scheuplein, 1967; Pirot *et al*, 1997). With $z/R << 1$, where z and R are the skin depth and the skin diffusion area radius, respectively, and with the donor solution-imposed concentration gradient in the z-direction, the mathematical expression for multidimensional transport can be simplified to one dimension (Deen, 1998).

Currently, experimental methods are not available to determine directly the permeant diffusion coefficient in the skin *in vitro*, and SC models have relied on measurements of diffusion coefficients in liposomes of various lipid compositions (Johnson *et al*, 1996a). In this study, we will focus on the oleic acid enhancer induced changes in the relevant transport properties discussed above, relative to the experimental control (without the enhancer), for each probe examined. The quantification of the relative change for each transport property under investigation is reported as an enhancement factor, E, which is the ratio of the value of the transport property with and without the chemical enhancer. From TPM data, the relative change in the vehicle to skin partition coefficient for each probe can be directly determined. Consequently, the relative change in the probe diffusion coefficient due to oleic acid enhancer action can be calculated using the following expression relating the probe flux, J, to its permeability, P (Schaefer and Redelmeier, 1996):

$$P = J/\Delta C \tag{2}$$

where $\Delta C$ is the difference in the probe concentration between the donor and the receiver compartments of the side-by-side diffusion cell used to measure P. For a given value of $\Delta C$, the permeability enhancement, $E_P$, which is the ratio of the permeant permeability in the presence of the chemical enhancer and that of the control (without the chemical enhancer), can be obtained by using Eqn 2 in Eqn 1, and then taking the ratio of the resulting expression for the chemical enhancer (E) and the control (C) samples. Specifically,

$$E_P = \frac{D_E}{D_C}\left(\frac{\left(\frac{dC}{dz}\right)_E}{\left(\frac{dC}{dz}\right)_C}\right) \tag{3}$$

where the first derivative, or the slope, of the linear permeant concentration profile (discussed later) established in the SC at steady-state conditions is a constant quantity. Note that $E_P = P_E/P_C$ can be calculated from the ratio of the measured transdermal permeabilities of each permeant at the two conditions (E and C) examined. Recall that, in general, the permeant permeability can be obtained as follows:

$$P = \frac{1}{A\Delta C}\left(\frac{dN}{dt}\right)_r \tag{4}$$

where $(dN/dt)_r$ is the change in the amount of permeant over time in the receiver compartment, and A is the area of the skin exposed to the donor solution. Moreover, for the steady-state transport of a permeant through biologic membranes, the permeant partition coefficient between the donor solution and the skin, K, and the skin barrier diffusion length, l, also play significant parts in determining the magnitude of the permeability coefficient, P. Specifically (Schaefer and Redelmeier, 1996),

$$P = \frac{KD}{l} \tag{5}$$

Using Eqn 5, one can express the permeability enhancement, $E_P$, in the following alternate useful form:

$$E_P = \frac{P_E}{P_C} = \frac{E_K E_D}{E_l} \tag{6}$$

where the partition-coefficient enhancement, $E_K$, the diffusion-coefficient enhancement, $E_D$, and the skin barrier diffusion length enhancement, $E_l$, are given, respectively, by

$$E_D = \frac{D_E}{D_C} \tag{7}$$

$$E_K = \frac{K_E}{K_C} \tag{8}$$

and

$$E_l = \frac{l_E}{l_C} \tag{9}$$

Substituting Eqn 3 in Eqn 6, the skin barrier diffusion length enhancement, $E_l$, can be expressed in the following useful form:

$$E_l = \frac{E_K}{E_g} \tag{10}$$

where

$$E_g = \frac{\left(\frac{dC}{dz}\right)_E}{\left(\frac{dC}{dz}\right)_C} \tag{11}$$

is the concentration-gradient enhancement. Equation 10 allows the calculation of the skin barrier diffusion length enhancement, $E_l$, utilizing quantities that are readily available through TPM experi-

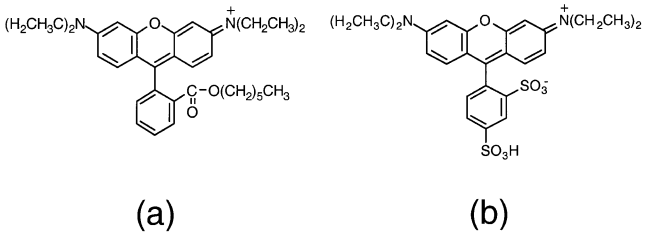


**Figure 2. Chemical structures of the two fluorescent model drugs examined.** (*a*) RBHE is the hydrophobic model drug, and (*b*) SRB is the hydrophilic analog. The two molecules are similar in molecular weight, 627 Da and 559 Da, respectively, but are distinguished by functional groups that impart drastic differences in octanol–PBS partition coefficients, $K_{O/PBS}$. RBHE lacks the two $SO_3^-$ groups present in SRB, but the hexyl ester group contributes to the higher $K_{O/PBS}$ values measured for RBHE compared with SRB (see **Table I**).

ments. Indeed, as shown below, both the concentration-gradient enhancement, $E_g$, and the partition-coefficient enhancement, $E_K$, can be extracted solely from the data obtained from the TPM three-dimensional scans of the fluorescent probe spatial distributions to determine the skin barrier diffusion length enhancement, $E_l$, which describes the relative change in the thickness of the permeant diffusion barrier in the z-direction resulting from the chemical enhancer action.

## MATERIALS AND METHODS

**Preparation of skin sample for imaging** Full-thickness human cadaver skin from the abdominal area (National Disease Research Interchange, Philadelphia, PA), acquired 10–20 h post mortem, was stored at −80°C and utilized within 3–6 wk. Upon use, the skin was thawed at room temperature (25°C), and the fat from the dermal side was removed. Skin samples of 2.25 $cm^2$ were mounted in side-by-side diffusion cells (9 mm diameter, PermeGear, Riegelsville, PA), and then immersed in phosphate-buffered saline (PBS; 0.01 M phosphate buffer, 0.0027 M KCl and 0.137 NaCl, pH = 7.4; Sigma, St Louis, MO) for the measurement of skin conductivities.

**Skin conductivity measurements** Skin conductivities for all the skin samples examined were measured as an indicator of the skin barrier integrity (Kontturi *et al*, 1993; Peck *et al*, 1994; Kalia and Guy, 1995). Ag–AgCl electrodes (E242, In Vivo Metric, Healdsburg, California) were connected to an AC signal generator (HP 33120A 15 MHz Function Arbitrary Waveform Generator, Hewlett Packard, Palo Alto, California) in series with a digital multimeter (Radio Shack, Fort Worth, TX). One electrode was placed in each compartment of the diffusion cell, filled with PBS, and a voltage drop of 100 mV was applied across the skin. To a 10 Hz current reading, the conductivity criterion of $> 10\ k\Omega\ cm^2$ was applied (Rossel *et al*, 1988), with skin samples not meeting this criterion replaced by intact skin.

**Fluorescent probe properties** The two fluorescent probes (Molecular Probes, Eugene, OR), rhodamine B hexyl ester perchlorate (RBHE) and sulforhodamine B (SRB), served as the hydrophobic and hydrophilic model drugs, respectively, and were selected based on their similarity in molecular structure, disparity in octanol–water partition coefficient, and fluorescence emission range. **Figure 2**(***a***,***b***) show the chemical structures of the two fluorescent probes, with their molecular weights (MW), fluorescence absorption (ab) and emission (em) spectral peaks (ab/em), and log $K_{O/PBS}$ (where $K_{O/PBS}$ is the experimentally determined octanol–PBS partition coefficient) listed in **Table I**. Whereas similar in structure, slight differences in the functional groups of RBHE and SRB result in octanol–PBS partition coefficients that vary by three orders of magnitude. The absence of the sulfate groups ($SO_3^-$) and the addition of the hexyl ester moiety ($C_6H_{13}COO$) in RBHE, compared with SRB, impart a greater tendency for hydrophobic interactions. The log $K_{O/PBS}$ values measured for RBHE and SRB are 2.49 and −0.45, respectively, clearly reflecting their roles as the hydrophobic and hydrophilic model drugs.

In addition to their physicochemical properties, these two probes were selected to minimize the effects of the skin autofluorescence, characterized by absorption and emission peaks of 488 nm and 515 nm, respectively (Masters *et al*, 1997). Specifically, under the 780 nm laser excitation, the fluorescence signals of the probes, their spectral absorption/emission peaks at 556 nm/578 nm (RBHE) and 565 nm/586 nm (SRB), have minimal overlap with that corresponding to the skin autofluorescence. Photon counts at each depth of the skin samples, kept in contact with the vehicles and in the absence of any fluorescent probes, maintained an average value of 1 and lower, with SD of up to 3 photon counts. These values clearly indicate that the signal detected in the presence of the fluorescent probe does indeed originate from the fluorescent probe alone, as the samples exposed to the fluorescent probes yielded average photon counts that are greater by two orders of magnitude.

**Table I. Fluorescent probe properties of the hydrophobic (RBHE) and hydrophilic (SRB) model probes examined**[a]

| Probe | RBHE | SRB |
|---|---|---|
| MW (Da) | 627 | 559 |
| ab/em (nm) | 556/578 | 565/586 |
| log $K_{O/PBS}$[b] | 2.49 ± 0.18 | −0.45 ± 0.0045 |

[a]The chemical structures of RBHE and SRB are illustrated in **Fig 2**(***a***,***b***), respectively. MW, molecular weight of each probe; ab/em, the probe spectral absorption (ab) and emission peaks (em); log $K_{O/PBS}$, measured values of the log of the probe PBS–octanol partition coefficients (described in the *Materials and Methods* section).
[b]Values are reported as mean ± SD. Experiments were performed in triplicate.

**Donor solution preparation** Donor vehicle solutions of RBHE and SRB consisting of ethanol (100%, Pharmco Products, Brookfield, CT) and PBS (Sigma, St Louis, MO), at a 1 : 1 ratio, by volume, were prepared at concentrations of 0.5 mg per ml and 0.7 mg per ml, respectively. In preparing the solutions containing the model chemical enhancer, an additional 5% by volume of oleic acid (99%, Sigma) was added to the PBS/ethanol probe solutions. Skin samples were left in contact with well-stirred donor solutions for 48 h, until the steady-state diffusion profile was established.

**Measurement of final skin conductivities** The final skin conductivities of the samples were again measured as described above to determine the changes in the skin barrier function due to chemical enhancer action, as conductivity measurements have frequently served as a useful indicator of the skin barrier function, and conductivity increases have similarly been found to correlate well with permeant permeability increases (Sims *et al*, 1991). Compared with the skin samples for which no changes in conductivity were measured after 48 h of contact with only PBS (the control case—no chemical enhancer), the skin samples treated with the oleic acid chemical enhancer indeed lowered the skin barrier function. The measured changes in skin conductivities for the samples kept in contact with the oleic acid solution are comparable with the 100–200-fold skin conductivity increases cited in the literature for skin treated with chemical enhancers (Inamori *et al*, 1994; Li *et al*, 1998).

**Skin preparation for TPM imaging** Each skin sample was then removed and rinsed with PBS/ethanol (1 : 1, by volume) and blotted with a Kimwipe (Kimberly Clark, Roswell, GA) to ensure the removal of any excess fluorescent probes present on the surface of the skin. The circular area of the skin exposed to the probes was cut out with a surgical carbon steel razor blade (VWR Scientific, Media, PA), and then sealed in an imaging chamber (2.5 mm Coverwell, Grace Bio-Laboratories, Bend, OR) with a no. 1, 22 mm square coverslip (VWR Scientific, Media, PA) contacting the SC side. A drop of PBS was added to the chamber to prevent the sample drying out.

**Permeability measurements** Control (no chemical enhancer) and chemical enhancer solutions of RBHE and SRB, prepared as described above, were radiolabeled with the equivalent tritiated probe (American Radiolabeled Chemicals, St Louis, MO) at 1 μCi per ml. Following the procedure described in the literature, the permeability measurements were performed (Johnson *et al*, 1996a) in triplicate using heat-stripped skin (Peck *et al*, 1994; (Li *et al*, 1998) with each of the four probe-vehicles, RBHE-control, RBHE-enhancer, SRB-control, and SRB-enhancer, serving as the donor solution for each set of experiments. The skin conductivities were measured before and after the experiments, as described above for each sample examined. The presence of radiolabeled permeants was detected with a liquid scintillation analyzer (2200CA Tri-

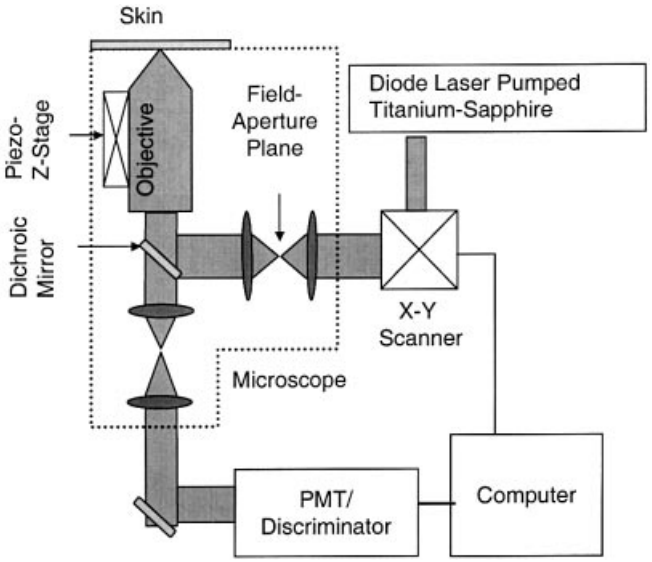


**Figure 3. Schematic illustration of the TPM.** Based on a point-scanning approach, the instrument utilizes a tight focal spot in three-dimensional imaging. Incident beams of light emitted from the diode laser pumped titanium-sapphire are deflected by the X–Y scanner to different angular positions, and then directed to the microscope system (area enclosed by the dotted lines). From the field-aperture plane, the laser is reflected from the dichroic mirror to the microscope objective. The skin sample is placed below the microscope objective, with the piezo-z stage controlling the scanner in the z-direction. Signal photons from the sample are processed with the photomultiplier tube/discriminator, and data analysis is performed with the computer.

Carb, Packard Instrument Company, Downers Grove, IL), and the steady-state permeant permeabilities were calculated utilizing Eqn 4.

**Determination of probe octanol–PBS partition coefficients** To obtain a calibration curve of fluorescence intensity *vs* concentration, solutions of varying concentrations were prepared by diluting the stock for each fluorescent probe. The fluorescence intensity at each known probe concentration was then measured with a fluorescence system (Photon Technology International, Monmouth Junction, NJ).

Two milliliters of each probe solution in PBS (≈ 0.05 mg per ml for RBHE and ≈ 0.07 mg per ml for SRB) were vortexed for 30 s with 2 ml of octanol (Fisher Scientific, Pittsburgh, PA) in a glass vial. Experiments were performed in triplicate. The vortexed mixtures were then allowed to equilibriate for 24 h. The aqueous phases were measured with the fluorescence system and the corresponding concentration was determined utilizing a calibration curve of probe concentration *vs* probe fluorescence intensity. Following the measurement of the initial and final probe concentrations in the aqueous phase, the quantity of probe in the octanol phase was determined by the difference between the initial and final concentrations of the aqueous phase. The probe octanol–PBS partition coefficient was calculated by taking the ratio of the final probe concentration in the octanol phase and that in the PBS phase. The octanol–PBS partition coefficients obtained here ($\log K_{O/PBS} = 2.49 \pm 0.18$ and $-0.45 \pm 0.0045$ for RBHE and SRB, respectively; see **Table I**) illustrate that for the concentrations used, SRB and RBHE act as the model hydrophilic and lipophilic molecules, respectively.

**Two-photon microscope** The TPM instrument used in this study is shown in **Fig 3**, with a general description of the instrumentation located elsewhere (So *et al*, 1998). In these studies, a femtosecond titanium-sapphire laser (Tsunami, Spectra-Physics, Mountain View, CA) pumped by a 5 W diode-pumped, solid-state continuous wave (CW) laser (Millennia, Spectra-Physics, Mountain View, CA) provided the two-photon excitation at 780 nm. The microscope system consisted of a modified inverted microscope (Axiovert 100TV, Zeiss, Thornwood, NY), a 40 × objective lens (Zeiss F Fluar, NA 0.13), and an objective micropositioner (model p-721 PIFOC, Physik Instrumente, Germany). X–Y scans are achieved using a scanner unit (Cambridge Technology, Watertown, MA), and photon pulses from the photomultiplier are discriminated against dark noise with an amplifier-discriminator unit (model F-100T, Advanced Research Instrument Corporation, Boulder, CO).

**Table II. Linear regression results for the sample average intensity profiles of the skin samples examined[a]**

| Probe | dI/dz (counts per μm) | $R^2$ |
|---|---|---|
| RBHE (C) | −7.66 ± 0.21 | 0.99 |
| RBHE (E) | −41.16 ± 1.67 | 0.99 |
| SRB (C) | −8.37 ± 0.38 | 0.98 |
| SRB (E) | −10.42 ± 0.58 | 0.97 |

[a]The reported intensity gradients, dI/dz, are the slopes of the SAIP corresponding to the first 8 μm of each skin sample examined, and were obtained from linear regressions (see *Materials and Methods*). The control and enhancer vehicles are denoted by (C) and (E), respectively. The error reported for dI/dz reflects the range of intensity gradient values that fall within a 95% confidence level based on the precision of the linear fit.

**Data collection** Per skin sample, four to six TPM scans of the fluorescence probe spatial distributions at different skin coordinates, or skin sites, were collected for each of the four treated skin samples (RBHE-control, RBHE-enhancer, SRB-control, and SRB-enhancer). The laser power (≈ 2 mW) was adjusted such that the fluorescence intensity emitted by the sample remained below the detection saturation threshold. The signal detection saturation threshold, below which a linear correlation exists between the fluorescence counts detected and the quantity of fluorescent probe present in the sample, was determined utilizing standard probe solutions of known concentrations.

**Data analysis** Three-dimensional images of the TPM data were examined with Spyglass Slicer (Spyglass, Inc., Lexington, MA) data visualization software on a personal computer (Dimension XPS D300, Dell, Round Rock, TX). A corresponding average probe fluorescence spatial distribution profile was calculated with an in-lab subroutine (Eric Ho, Massachusetts Institute of Technology, Cambridge, MA) for each three-dimensional scan. At each depth (z-coordinate) scanned, the subroutine averages the fluorescence counts associated with the pixels in the 256 by 256 pixel image representing the imaged field. For each site analyzed by the subroutine, a plot of the average fluorescence count *vs* the corresponding skin depth generates the site-specific average fluorescent probe spatial distribution profile (SSDP), which is the quantitative representation of the three-dimensional visualization generated with Spyglass Slicer.

**Generation of fluorescent probe intensity profiles** Per skin sample, the surface of each of the four to six sites examined, corresponding to $z = 0$ μm, was defined by the scanning depth yielding the highest average fluorescence count. The definition of these surfaces normalized the different SSDP and enabled the subsequent calculation of the sample average intensity profile (SAIP) for each probe-vehicle combination based on the four to six sites surveyed. In calculating each SAIP, the fluorescence counts associated with each individual SSDP corresponding to a given z-coordinate were averaged. This average was then plotted *vs* the corresponding z-coordinate to yield the SAIP, I(z). The calculated SD from the SAIP represent the site to site variations in probe penetration within a particular skin sample.

**Fluorescent probe intensity gradient calculation** The intensity gradient (or the slope) corresponding to each SAIP was calculated by performing a linear regression for the data points comprising the first 11 axial scans, or 8 μm, of the skin, a region encompassing the drastic decrease in probe intensity for the control cases (in the absence of chemical enhancer) to which chemical enhancer-induced changes in probe transport are compared. The error in the intensity gradient corresponding to each SAIP is expressed as the range in which a 95% confidence level exists (see **Table II**).

Because of the direct correlation between the probe fluorescence intensity and the probe concentration established with the standard probe solutions described above, the shape of the SAIP provides a good representation of the probe concentration profile in the skin sample. Hence, the calculation of the concentration-gradient enhancement, $E_g$, for each probe results from substituting the values of dI/dz, listed in **Table II**, for those of the corresponding probe concentration gradients, dC/dz (see Eqn 11).

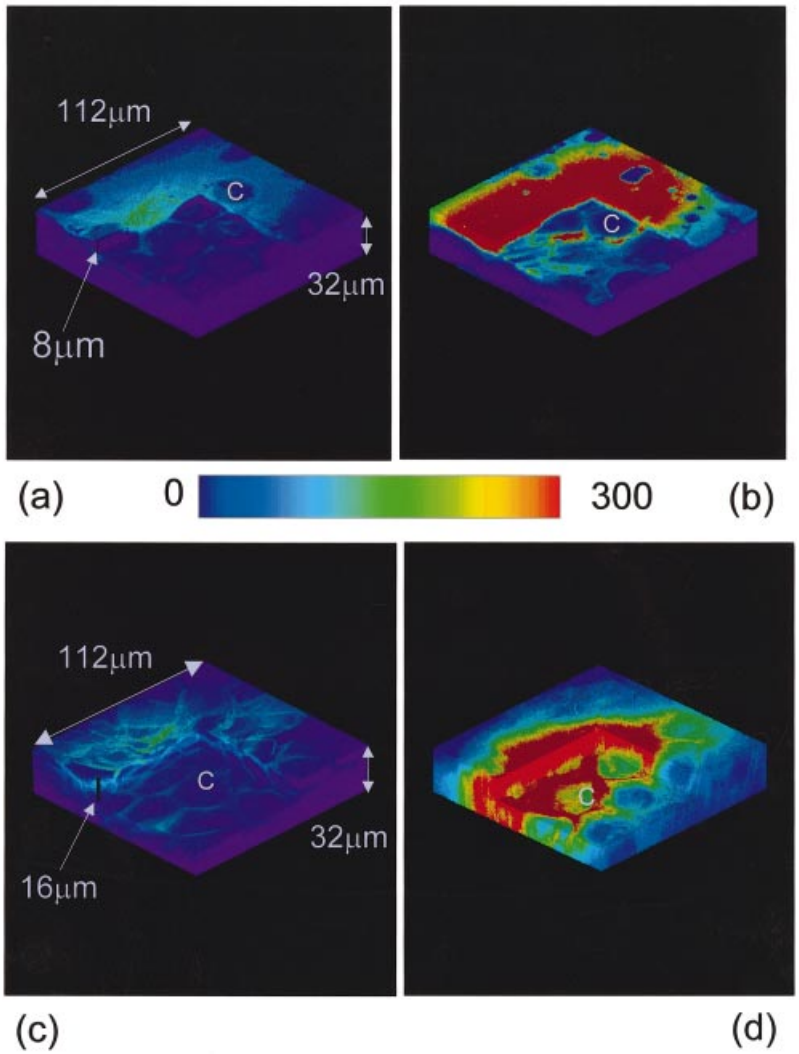


**Figure 4. Three-dimensional probe distributions in the upper 32 μm of the skin sample.** (*a,b*) Depict the hydrophobic probe (RBHE) spatial distributions resulting from the control and the chemical enhancer vehicles, respectively. (*c,d*) Depict the hydrophilic probe (SRB) spatial distributions resulting from the control and the chemical enhancer vehicles, respectively. To highlight the structural features, quadrants of 8 and 16 μm in depth are removed from the respective probe distribution images, as shown by the length scales drawn on the control samples for each probe. The color scale indicates an increase in probe concentration as the colors progress from 0 to 300.

Moreover, the intensity gradient of each SSDP was calculated in the same manner, and then averaged to assess the relationship between the sample average intensity gradient and the corresponding site-specific intensity gradient.

**Quantification of changes in the probe vehicle to skin partition coefficient** For each probe, the concentration difference between the donor and the receiver diffusion cell compartments, $\Delta C$ (see Eqn 2), was approximated by the probe donor concentration $C_d$ because $C_d/C_r \gg 1$, where $C_r$ is the probe concentration in the receiver compartment. Hence, under these infinite sink conditions, $C_d$ remains a fairly constant quantity in the control and the chemical enhancer permeability studies for both SRB and RBHE.

With a constant $C_d$ value for the control and the enhancer solutions for each probe, and given that $K = C_s|_0/C_d$ (Schaefer and Redelmeier, 1996), where K is the probe vehicle to skin partition coefficient and $C_s|_0$ is defined as the probe concentration in the skin at the surface (at $z = 0$ μm) (Pirot *et al*, 1997; Deen, 1998), the probe vehicle to skin partition-coefficient enhancement, $E_K$, was approximated for each probe by taking the ratio of the average fluorescence intensity at the skin surface (corresponding to $z = 0$ μm) for the enhancer and the control samples. Specifically,

$$E_K = \frac{I_E(z)\,|_{z=0}}{I_C(z)\,|_{z=0}} \qquad (12)$$

where $I_E(z)$ and $I_C(z)$ represent the average intensities of the probe for the enhancer and the control cases, respectively. For these studies, the skin volume associated with the concentration of the probe detected at the skin surface corresponds to the volume defined by the area of the field scanned and the two-photon laser beam point size in the axial or z-direction. Because the relative change in the probe vehicle to skin partition coefficient is the quantity of interest here, for the same skin surface volume, only the average probe surface intensity is considered.

## RESULTS

**Three-dimensional visualization of fluorescent probe spatial distributions in the skin** To illustrate the qualitative details that one can obtain using the TPM z-scans, representative three-dimensional images of the probe spatial concentration (or intensity) distributions for one site of the four sites examined per skin sample are shown in **Fig 4**(***a–d***). Each three-dimensional construct represents a field of 112 × 112 μm and a depth of 32 μm from the surface of the skin. The color scales used for these images are also shown in **Fig 4**, where regions in red (corresponding to 300) reflect regions of high probe concentration and regions in blue (corresponding to 0) reflect regions of low probe concentration. The C in each part of the figure points to structures resembling corneocytes.

*Hydrophobic probe RBHE* **Figure 4**(***a,b***) illustrates the spatial distributions of the hydrophobic probe RBHE across the thickness of the skin sample (32 μm) without (the control) and with the chemical enhancer oleic acid, respectively. Illustrating that the SC acts as the primary barrier to transdermal transport, the majority of the drop in intensity for RBHE occurs over the

uppermost layers of the skin, approximately over 10 μm, limiting the fluorescence signal detection beyond that depth (see **Fig 4*a,b***).

*Hydrophilic probe SRB* **Figure 4(*c,d*)** illustrates the spatial distributions of the hydrophilic probe SRB across the skin sample (32 μm). For the hydrophilic probe, SRB, in the control condition (see **Fig 4*c***), the majority of the drop in probe intensity also occurs in the uppermost layers of the skin. In the presence of the oleic acid enhancer, however, the gradual decline of SRB concentration across the SC and into the VE (see **Fig 4*d***) suggests that the chemical enhancer has reduced the SC barrier properties such that the contribution of the VE to the overall skin barrier becomes more noticeable.

*Similarities between RBHE and SRB* For both RBHE and SRB, the presence of oleic acid is qualitatively observed to increase the quantity of each probe on the surface of the skin (cf. **Fig 4*a*** and **Fig 4*b*** for RBHE, and **Fig 4*c*** and **Fig 4*d*** for SRB), which is indicative of increased partitioning of the probe into the skin. Moreover, the quantities of RBHE and SRB detected in the control samples are significantly lower as they lie in the blue region of the color scale (see **Fig 4*a,c***). Increases in both the partition coefficient and the concentration gradient of the probe due to the presence of oleic acid should contribute to an increase in the overall transdermal transport of the probe, as described by Eqns 1 and 5.

Based on these three-dimensional images, regions of high probe concentration surround the corneocytes, suggesting that the primary transport pathway across the skin is through the lipid multilamellar regions between the corneocytes for both the hydrophobic and the hydrophilic model drugs examined. Because the resolution of these two-photon microscope images is limited by the laser scanning spot size of ≈1 μm, molecular scale details are not visually accessible. Nevertheless, as discussed above and shown below, changes in the transport microenvironment can be inferred from a quantification of these images.

*Differences between RBHE and SRB* Although both the hydrophobic and the hydrophilic model drugs examined appear to traverse the skin primarily via the intercellular route, the differences observed in the nature of the probe spatial distributions throughout the skin samples suggest that oleic acid enhancer action operates through different mechanisms for these two model drugs. These qualitative differences include the pronounced decrease observed in the average intensity for the hydrophobic probe over the first 8 μm of the skin sample, represented by the changes in the color scale from green to blue and from red to blue (see **Fig 4*a,b***), for the control and the enhancer samples, respectively. A similar decrease in probe fluorescence signal, from green to blue (see **Fig 4*c***), was detected for the hydrophilic probe over the first 16 μm in the control skin sample, but its spatial distribution in the presence of oleic acid enhancer changed, showing the perfusion of hydrophilic probe throughout the 32 μm of the skin sample (see **Fig 4*d***), highlighted by the regions in red. Insight into these differences in transport mechanisms can be gained from a more quantitative analysis of the two-photon data, which is presented next.

**Quantification of the fluorescent probe spatial distributions in the skin** **Figures 5** and **6** show the measured average photon counts *vs* skin depth, representing the respective average concentration profiles of the hydrophobic (RBHE) and the hydrophilic (SRB) model drugs as described in the *Materials and Methods* section. (The estimated instrumentation error in the z direction is 5%.) The average intensity profile at the skin surface (z = 0 μm) is proportional to the magnitude of the probe skin–vehicle partition coefficient, and the slope of the curve corresponds to the probe concentration gradient.

*Quantification of the relative change in the probe vehicle–skin partition coefficient, $E_K$* The higher probe concentrations detected at the surfaces of the three-dimensional representations of the oleic acid treated samples (see **Fig 4*b,d***) agree with their corresponding probe intensity profiles in which 4-fold increases in the average photon

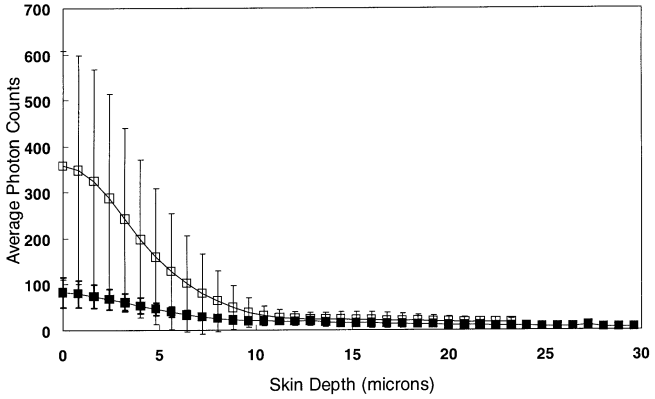


**Figure 5. Sample average intensity profiles of RBHE.** Key: sample average intensity counts calculated at each depth for the control (■) and the enhancer (□) vehicles. The average photon counts is plotted *vs* the corresponding skin depth. The error bars indicate 1 SD from the sample average intensity of the five and six different sites sampled for each condition, respectively.

counts are measured at z = 0 μm (cf. □ and ■ in **Figs 5** and **6**). A calculation of the probe partition-coefficient enhancement, $E_K$, utilizing the $I_E$ and $I_C$ values obtained from the SAIP at z = 0 μm, yields values of 4.33 ± 3.45 and 4.56 ± 2.05 for the hydrophobic and the hydrophilic probes, respectively. The partitioning of both the hydrophobic and the hydrophilic probes from the control solution (1 : 1 PBS/ethanol) into the skin is enhanced to a similar degree in the presence of the oleic acid enhancer. For both probes, the large error in $E_K$ arises from the site to site variation of the probe average fluorescence profiles, as seen in **Figs 5** and **6**, in which the error bars reflect the variation in the SSDP detected at each skin depth (z-coordinate). The deduced $E_K$ values further substantiate the increased partitioning of both RBHE and SRB from the vehicle to the skin in the presence of the oleic acid chemical enhancer shown in **Fig 4*b*** and ***d***, respectively.

*Quantification of the relative change in the probe intensity gradient, $E_g$* In addition to the partition-coefficient enhancement, the intensity gradients were calculated (see *Materials and Methods* section) for the SAIP in **Figs 5** and **6**, and the results are reported in **Table II** with respect to the slope and $R^2$ corresponding to the linear regression. The error corresponding to the slope calculations represents the statistical range in which a 95% confidence level exists. As expected from the SAIP, the intensity gradients for RBHE and SRB in the control vehicles are similar, with values of −7.66 ± 0.21 counts per μm and −8.37 ± 0.38 counts per μm, respectively; however, the presence of the oleic acid enhancer significantly increases the steepness of the intensity gradient of RBHE (dI/dz = − 41.16 ± 1.67 counts per μm), while having little effect on the SRB intensity gradient (dI/dz = − 10.42 ± 0.58 counts per μm). Based on the slope values determined, the concentration-gradient enhancements are $E_g$ = 5.37 ± 0.26 for RBHE and $E_g$ = 1.24 ± 0.09 for SRB, indicating that the RBHE flux enhancement results from an increase in the concentration gradient, one of the factors driving permeant flux across the skin (see Eqn 1), as well as by increased probe partitioning into the skin.

*Quantification of site-specific probe intensity gradients* The average intensity gradients calculated from the SAIP were compared with the intensity gradients obtained from each specific site examined by performing a linear regression of the SSDP. The four to six SSDP (not shown) that generate each SAIP revealed variations in probe intensity at each depth that were twice as large as those observed at the corresponding depth of the SAIP. These statistics suggest that the error bars associated with each SAIP may be reduced with increased sampling of different sites on the skin sample. Based on the statistics of a normal distribution, the error associated with each

**Table III. SSDP linear regression results for each site examined[a]**

| | RBHE | | | | SRB | | | |
|---|---|---|---|---|---|---|---|---|
| Site no. | dI/dz (C) | $R^2$ | dI/dz (E) | $R^2$ | dI/dz (C) | $R^2$ | dI/dz (E) | $R^2$ |
| 1 | –3.18 | 0.99 | –20.30 | 0.97 | –6.60 | 0.98 | –22.03 | 1.00 |
| 2 | –5.93 | 0.99 | –20.30 | 0.98 | –10.48 | 0.94 | –16.63 | 1.00 |
| 3 | –13.00 | 0.96 | –52.80 | 0.96 | –12.71 | 0.98 | –15.53 | 0.98 |
| 4 | –9.42 | 0.98 | –88.70 | 0.98 | –8.82 | 1.00 | –10.11 | 1.00 |
| 5 | –6.78 | 0.99 | –40.60 | 0.95 | – | – | –12.84 | 1.00 |
| 6 | – | – | –24.29 | 0.95 | – | – | – | – |
| AVG[b] | –7.66 ± 3.72 | | –41.17 ± 26.65 | | –9.65 ± 2.58 | | –15.43 ± 4.47 | |

[a]The linear regression for each SSDP was performed for the first 11 axial scans at each site to obtain the intensity gradient, dI/dz. The value of dI/dz for each site is reported for the control (C) and enhancer (E) cases. The $R^2$ value following each reported dI/dz value describes the accuracy of the linear fit.
[b]For each group of SSDP, the average value, AVG, of the intensity gradients calculated for the respective number of sites imaged per skin sample is reported as the mean ± SD.

SAIP should decrease by the square root of the number of SSDP utilized in the analysis.

**Table III** reports the individual site-specific probe intensity gradient values followed by the average of those values for each of the SSDP belonging to each of the four cases examined (RBHE-control, RBHE-enhancer, SRB-control, and SRB-enhancer). The control and enhancer cases corresponding to RBHE for the SAIP intensity gradient (– 7.66 ± 0.21 and –41.16 ± 1.67) and the average of the SSDP intensity gradients (– 7.66 ± 3.72 and –41.17 ± 26.65) revealed nearly identical means. Whereas the averages of the SSDP intensity gradients (– 9.65 ± 2.58, control; –15.43 ± 4.47, enhancer) calculated for SRB were, in general, more negative in value than the corresponding SAIP intensity gradients (– 8.37 ± 0.38, control; –10.42 ± 0.58, enhancer), the differences between the two intensity gradient calculations are ultimately captured within their error bars. The analysis of the SSDP intensity gradients presented above suggests that the application of the SAIP in the methodology introduced here serves as an average representation of the different SSDP sampled**.**

A discussion of the changes in the skin barrier diffusion length and the skin diffusion coefficient of the permeant deduced from the permeability enhancement, $E_P$, concentration-gradient enhancement, $E_g$, and partition-coefficient enhancement, $E_K$, for RBHE and SRB is presented below.

**Quantification of oleic acid-induced changes in transdermal transport properties** The enhancements of the concentration gradient, $E_g$, vehicle to skin partition coefficient, $E_K$, permeability coefficient, $E_P$, skin barrier diffusion length, $E_l$, and diffusion coefficient, $E_D$, are shown in **Fig 7**. The error bars represent 1 SD from the average value, except for $E_g$, for which the error bars indicate a 95% confidence level in the results (described in *Materials and Methods*). Factors contributing to the enhanced permeability values for the hydrophilic probe ($E_P$ = 9.59 ± 2.92) and the hydrophobic probe ($E_P$ = 7.35 ± 1.00) are immediately revealed by the $E_g$ and $E_K$ values. The $E_g$ values corresponding to the probe concentration gradients increased by 5.37 ± 0.26 (gray bar in **Fig 7**) and 1.24 ± 0.09 (striped bar in **Fig 7**), for the hydrophobic (RBHE) and the hydrophilic (SRB) probes, respectively. Despite the negligible change in the concentration gradient obtained for SRB in the presence of oleic acid, the value for $E_K$ (4.56 ± 2.05, striped bar in **Fig 7**) suggests that the main driving force for flux enhancement in this case is due to the SRB increased affinity for the SC.

As shown in **Fig 6**, the average intensity profile for SRB maintains a similar shape in both the presence and the absence of oleic acid, but is translated in the direction of increasing intensity by a factor of 4 in the presence of oleic acid. For RBHE, both $E_g$ and $E_K$ clearly indicate increases in the average concentration gradient and skin partitioning in the presence of oleic acid with values of 5.37 ± 0.26 and 4.33 ± 3.45 (gray bars in **Fig 7**), respectively.

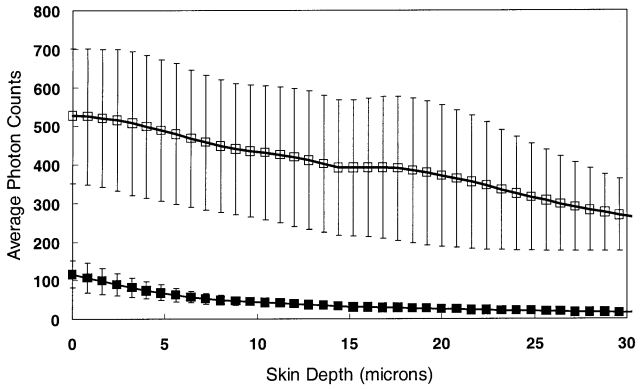


**Figure 6. Sample average intensity profiles of SRB.** Key: sample average intensity counts calculated at each depth for the control (■) and the enhancer (□) vehicles. The average photon counts is plotted *vs* the corresponding skin depth. The error bars indicate 1 SD from the sample average intensity of the four and five different sites sampled for each condition, respectively.

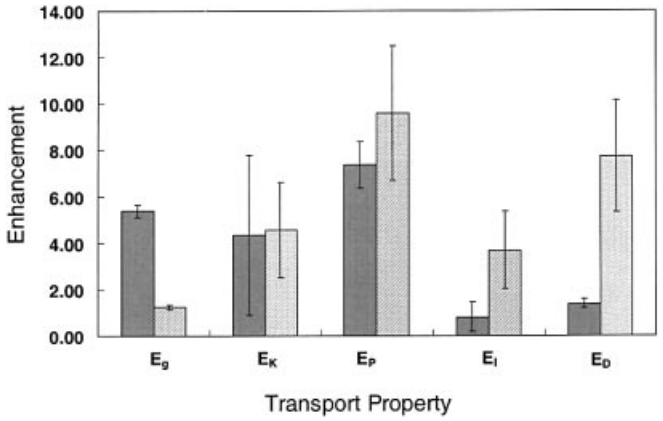


**Figure 7. Relative changes in transport parameters.** Key: RBHE (gray bars), SRB (striped bars). With the exception of $E_g$, the error bars indicate 1 SD from the mean. The error bars corresponding to $E_g$ for both probes represent the upper and the lower limit of a 95% confidence level. The enhancement factors calculated for RBHE are: $E_g$ = 5.37 ± 0.26, $E_K$ = 4.33 ± 3.45, $E_P$ = 7.35 ± 1.00, $E_l$ = 0.81 ± 0.64, and $E_D$ = 1.37 ± 0.20. The enhancement values calculated for SRB are: $E_g$ = 1.24 ± 0.09, $E_K$ = 4.56 ± 2.05, $E_P$ = 9.59 ± 2.92, $E_l$ = 3.66 ± 1.67, and $E_D$ = 7.70 ± 2.41.

These results presented for both the hydrophilic and the hydrophobic probes are consistent with the two-layer transdermal diffusion model proposed by Yamashita *et al* (1995), who used

mannitol (polar) and 6-mercaptopurine (nonpolar) as the model drugs in a system that accounts for the existence of both a polar and a nonpolar permeant transport route through the SC. For both routes, their results showed that the oleic acid action increased their model parameter associated with permeant partitioning from the vehicle to the skin (Yamashita *et al*, 1995).

*Quantification of oleic acid-induced changes in the SC microtransport environment as reflected in $E_D$ and $E_l$* The oleic acid-induced changes in the hydrophilic probe microtransport environment that promote increased transdermal diffusion are discussed next. From the relative changes in the intensity gradient, $E_g$, and the skin partition coefficient, $E_K$, one can subsequently estimate the changes that arise in the permeant skin barrier diffusion length, reflected in $E_l$, and in the permeant skin diffusion coefficient, reflected in $E_D$. $E_l$ is calculated using Eqn 10, in which the permeant skin barrier diffusion length enhancement is simply the ratio of $E_K$ and $E_g$, the two enhancement factors readily obtained using the SAIP shown in **Figs 5** and **6**. By applying Eqn 6, in which $E_D$ can now be obtained as a function of $E_P$, $E_K$, and $E_l$ upon rearranging the equation, the quantitative changes in the permeant skin diffusion coefficient can be obtained.

For the hydrophilic probe, SRB, in the presence of oleic acid, an increase in the skin barrier diffusion length was calculated, as well as clearly visualized in **Fig 6** (□). Based on Eqn 5, an increase in the skin barrier diffusion length would contribute to a decrease in the permeability, but the concomitant increase in probe partition coefficient, $E_K = 4.56 \pm 2.05$, and diffusion coefficient, $E_D = 7.70 \pm 2.41$, offsets the increase in skin barrier diffusion length, $E_l = 3.66 \pm 1.67$

In contrast to the changes estimated for the microtransport properties of the hydrophilic probe, the skin barrier diffusion length and diffusion coefficient of the hydrophobic probe, RBHE, show minor deviations from the control condition in the presence of oleic acid, as reflected in the values of $E_l = 0.81 \pm 0.64$ and $E_D = 1.37 \pm 0.20$, respectively.

The deduced values for the both the skin barrier diffusion length enhancement and the diffusion-coefficient enhancement are discussed below, first for the hydrophilic probe, SRB, and subsequently for the hydrophobic probe, RBHE.

## DISCUSSION

**Implications of changes detected in the hydrophilic probe transport properties** The observed increase in the skin barrier diffusion length ($E_l = 3.66 \pm 1.67$) for the hydrophilic probe in the presence of oleic acid suggests the creation of a microtransport environment in the SC, which is more amenable to hydrophilic drug transport, such that the predominant skin barrier now includes both the SC and the viable epidermis. The precise significance of the 4-fold increase in the skin barrier diffusion length, with respect to the physical dimensions and structural components of the different skin layers, requires further investigation. As revealed by the increase in the diffusion coefficient ($E_D = 7.70 \pm 2.41$), the permeant microenvironment has noticeably changed to allow for the increased mobility of SRB. Therefore, the diffusion of the hydrophilic permeant exhibits a greater sensitivity to changes in the lipid environment because of its inherent incompatibility with the SC lipid environment under passive conditions. The increases measured for the vehicle to skin partition coefficient, the skin barrier diffusion length, and the diffusion coefficient reflect microenvironmental changes in the SC. The relationship between the microenvironmental changes reported here and the microscale descriptions of transport pathway changes noted in the literature, such as, increases in the hydrophilic permeant pathway pore sizes (Yamashita *et al*, 1995) as well as oleic acid phase separation and domain formation in the SC lipid region (Ongpipattanakul *et al*, 1991), requires further investigation.

**Implications of changes detected in the hydrophobic probe transport properties** Compared with the significant increase detected in the skin barrier diffusion length for the hydrophilic probe, the minor change in this value for the hydrophobic probe ($E_l = 0.81 \pm 0.64$) indicates that, even in the presence of oleic acid enhancer action, the SC comprises the primary barrier to transdermal transport, as the deeper layers of the skin do not contribute to the transport barrier delineated by the drop in the probe concentration across the first 8 μm of the skin. The minor effect of oleic acid on the microtransport environment of the hydrophobic probe, as reflected in the $E_D$ value of $1.37 \pm 0.20$, can be attributed to the natural intrinsic compatibility of the hydrophobic probe with the SC lipid environment.

The increase in SC lipid fluidity associated with oleic acid enhancer action, in this case, is primarily manifested by the increased partitioning of the hydrophobic molecule into the skin, reflected in $E_K = 4.33 \pm 3.45$, followed by the increased concentration gradient driving transdermal diffusion, reflected in $E_g = 5.37 \pm 0.26$. The error bars shown on the SAIP curves reflect the heterogeneity of the SC and result from the spread in the individual pixel intensities for each SSDP. We believe that these large variations (twice as large as those observed for the SAIP) in the SSDP are mainly dominated by the skin location morphologic variation on the micron scale. In the presence of oleic acid chemical enhancer action, the variance for both RBHE (**Fig 5**, □) and SRB (**Fig 6**, □), increases, as reflected in the increased size of the error bars relative to the control cases (**Figs 5** and **6**, ■). In light of this observation, additional variance may also result from the nonuniform action of the oleic acid. A heterogeneous distribution of oleic acid throughout the SC may result from the formation of separate domains of oleic acid pools within the SC lipids (Ongpipattanakul *et al*, 1991).

Based on the data presented, the variance due to SC morphology may be reduced by sampling over larger areas at each site in the skin sample; however, as the sampling area increases, the intrinsic heterogeneity of the skin properties and the nonuniform action of the oleic acid chemical enhancer may become more evident. Further studies over larger skin areas may enable us to address better the site to site variations observed in the skin model.

Moreover, the application of an alternative approach, where regions containing no probe (corneocyte regions) are excluded from the average intensity calculation, may provide information pertaining to the probe diffusion and distribution on the submicron scale. By evaluating only the probe-rich regions, this approach eliminates the morphology-dependent contribution to the spread in SSDP variations. Whereas the methodology applied in our studies has examined probe transport through a medium consisting of two different components (corneocytes and lipid multilamellae), the alternative analysis method focuses more specifically on transport through the continuous phase of the SC (the lipid regions). Hence, this approach decomposes the SC into its more fundamental components, and evaluates one aspect of the overall mechanism of transdermal transport. Future studies involving the rigorous comparison of results arising from the two data analysis schemes, as well as an increased sampling of skin sites, will provide additional insight into the mechanism of chemical enhancer action.

## CONCLUSIONS

The advantages of TPM in providing three-dimensional images detailing the chemical enhancer-induced changes in fluorescent probe distributions in the upper 32 μm of skin samples, with respect to important structural features such as the corneocytes and the lipid multilamellar region, have been demonstrated here. More importantly, we have presented here, for the first time, a methodology that quantitatively characterizes the significance of the visualized differences in these three-dimensional images with respect to the commonly investigated permeant transport parameters. The agreement between the apparent changes in probe concentration gradient, probe partitioning, probe diffusion coefficient, and probe skin barrier diffusion length, estimated using this method, and the phenomenologic explanations of permeability

enhancement detailed in the literature illustrates the potential of two-photon microscopy in elucidating the mechanisms of transdermal transport processes at the mechanistic level. The results presented above for this *in vitro* model system, in addition to the noninvasive nature of TPM, reinforces the potential applicability of utilizing this method in future studies to understand the changes underlying the experimentally measured permeabilities for *in vivo* systems.

*This research was supported by a National Institutes of Health Grant GM44884. We would like to thank Eric Ho and Evie Lee for their assistance in analyzing the two-photon microscopy data. Furthermore, we would like to thank Hua Tang for very useful discussions on various aspects of transdermal transport theory.*

## REFERENCES

Bommannan D, Potts RO, Guy RH: Examination of the stratum corneum barrier function in vivo by infrared spectroscopy. *J Invest Dermatol* 95:403–408, 1990

Cullander C, Guy RH: (D) Routes of delivery: case studies (6) Transdermal delivery of peptides and proteins. *Adv Drug Deliv Rev* 8:291–329, 1992

Deen WM: *Analysis of Transport Phenomena*. New York: Oxford University Press, 1998

Denk W, Strickler JH, Webb WW: Two-photon laser scanning fluorescence microscopy. *Science* 248:73–76, 1990

Denk W, Piston DW, Webb WW: Two-photon molecular excitation in laser-scanning microscopy. In: Pawley JB (ed.). *Handbook of Biological Confocal Microscopy*. New York: Plenum Press, 1995: pp 445–458

Diaspro A: Introduction to two-photon microscopy. *Microsc Res Tech* 47:163–164, 1999

Finnin BC, Morgan TM: Transdermal penetration enhancers: applications, limitations, and potential. *J Pharm Sci* 88:955–958, 1999

Francoeur ML, Golden GM, Potts RO: Oleic acid: Its effects on stratum corneum in relation to (trans)dermal drug delivery. *Pharm Res* 7(6):621–627, 1990

Golden GM, McKie JE, Potts RO: Role of stratum corneum lipid fluidity in transdermal drug flux. *J Pharm Sci* 76:25–28, 1987

Grewal BS, Naik A, Irwin WJ, Gooris G, Grauw CJD, Gerritsen HG, Bouwstra JA: Transdermal macromolecular delivery: real-time visualization of iontophoretic and chemically enhanced transport using two-photon excitation microscopy. *Pharm Res* 17:788–802, 2000

Guy RH: Current status and future prospects of transdermal drug delivery. *Pharm Res* 13:1765–1769, 1996

Inamori T, Ghanem A-H, Higuchi WI, Srinivasan V: Macromolecule transport in and effective pore size of ethanol pretreated human epidermal membrane. *Int J Pharm* 105:113–123, 1994

Johnson ME, Berk DA, Blankschtein D, Golan DE, Jain RK, Langer RS: Lateral diffusion of small compounds in human stratum corneum and model lipid bilayer systems. *Biophys J* 71:2656–2668, 1996a

Johnson ME, Mitragotri S, Patel A, Blankschtein D, Langer R: Synergistic effects of chemical enhancers and therapeutic ultrasound on transdermal drug delivery. *J Pharm Sci* 85:670–679, 1996b

Kalia YN, Guy RH: The electrical characteristics of human skin in vivo. *Pharm Res* 12:1605–1613, 1995

Kontturi K, Murtomaki L, Hirvonen J, Paronen P, Urtti A: Electrochemical characterization of human skin impedance spectroscopy: the effect of penetration enhancers. *Pharm Res* 10:381–385, 1993

Kuijk-Meuwissen MEMJv, Junginger HE, Bouwstra JA: Interactions between liposomes and human skin in vitro, a confocal laser scanning microscopy study. *Biochim Biophys Acta* 1371:31–39, 1998

Li SK, Suh W, Parikh HH, Ghanem A-H, Mehta SC, Peck KD, Higuchi WI: Lag time data for characterizing the pore pathway of intact and chemically pretreated human epidermal membrane. *Int J Pharm* 170:93–108, 1998

Mak VHW, Potts RO, Guy RH: Oleic acid concentration and effect in human stratum corneum: Non-invasive determination by attenuated total reflectance infrared spectroscopy. *J Control Rel* 12:67–75, 1990

Masters BR, So PTC, Gratton E: Multiphoton excitation fluorescence microscopy and spectroscopy of in vivo human skin. *Biophys J* 72:2405–2412, 1997

Masters BR, So PTC, Gratton E: Optical biopsy of in vivo human skin: Multiphoton excitation microscopy. *Lasers Med Sci* 13:196–203, 1998

Naik A, Pechtold LARM, Potts RO, Guy RH: Mechanism of oleic acid-induced skin penetration enhancement in vivo in humans. *J Control Rel* 37:299–306, 1995

Ongpipattanakul B, Burnette R, Potts RO, Francoeur ML: Evidence that oleic acid exists in a separate phase within stratum corneum lipids. *Pharm Res* 8:350–354, 1991

Peck KD, Ghanem A-H, Higuchi WI: Hindered diffusion of polar molecules through and effective pore radii estimates of intact and ethanol treated human epidermal membrane. *Pharm Res* 11:1306–1314, 1994

Peck KD, Hsu J, Lee SK, Ghanem A-H, Higuchi WI: Flux enhancement effects of ionic surfactants upon passive and electroosmotic transdermal transport. *J Pharm Sci* 87:1161–1169, 1998

Peck KD, Srinivasan V, Li SK, Higuchi WI, Ghanem A-H: Quantitative description of the effect of molecular size upon electroosmotic flux enhancement during iontophoresis for a synthetic membrane and human epidermal membrane. *J Pharm Sci* 85:781–788, 1996

Periasamy A, Skoglund P, Noakes C, Keller R: An evaluation of two-photon excitation versus confocal and digital deconvolution fluorescence microscopy imaging in *Xenopus* morphogenesis. *Microsc Res Tech* 47:172–181, 1999

Pirot F, Kalia YN, Stinchcomb AL, Keating G, Bunge A, Guy RH: Characterization of the permeability barrier of human skin in vivo. *Proc Natl Acad Sci USA* 94:1562–1567, 1997

Potts RO, Francoeur ML: The influence of stratum corneum morphology on water permeability. *J Invest Dermatol* 96:495–499, 1991

Pugh WJ, Hadgraft J, Roberts MS: Physicochemical determinants of stratum corneum permeation. In: Roberts MS, Walters KA (eds). *Dermal Absorption and Toxicity Assessment*. New York: Marcel Dekker, Inc., 1998: pp 91, 245–268

Rossel J, Colominas J, Riu P, Pallas-Areny R, Webster JG: Skin impedence from 1 Hz to 1MHz. *IEEE Trans Biomed Eng* 35:649–651, 1988

Schaefer H, Redelmeier TE: *Skin Barrier*. Basel: Karger, 1996

Scheuplein RJ: Mechanism of percutaneous absorption. *J Invest Dermatol* 48:79–88, 1967

Scheuplein RJ, Blank IH: Permeability of the skin. *Physiol Rev* 51:702–747, 1971

So PTC, Kim H, Kochevar IE: Two-photon deep tissue ex vivo imaging of mouse dermal and subcutaneous structures. *Optics Express* 3:339–359, 1998

Soeller C, Cannell MB: Two-photon microscopy: Imaging in scattering samples and three-dimensionally resolved flash photolysis. *Microsc Res Tech* 47:182–195, 1999

Turner NG, Guy RH: Iontophoretic transport pathways: Dependence on penetrant physicochemical properties. *J Pharm Sci* 86:1385–1389, 1997

Yamashita F, Koyama Y, Kitano M, Takakura Y, Hashida M: Analysis of in vivo skin penetration enhancement by oleic acid based on a two-layer diffusion model with polar and nonpolar routes in the stratum corneum. *Int J Pharm* 117:173–179, 1995

Yoneto K, Ghanem AH, Higuchi WI, Peck KD, Li SK: Mechanistic studies of the 1-alkyl-2-pyrrolidones as skin permeation enhancers. *J Pharm Sci* 84:312–317, 1995